

Thermal Protective Performance of Silica Aerogel Felt Bedded Firefighters' Protective Clothing under Fire Conditions

Dongmei HUANG^{1,2*}, Chenning GUO¹

¹ College of Quality and Safety Engineering, China Jiliang University, Hangzhou, Zhejiang, 310018, China

² Key Laboratory of Furniture Inspection Technology of Zhejiang Province, Hangzhou, Zhejiang, 310018, China

crossref <http://dx.doi.org/10.5755/j01.ms.23.4.16680>

Received 05 November 2016; accepted 18 March 2017

The addition of silica aerogel felt (SAF) to firefighters' protective clothing (FPC) is an innovation with the potential to enhance the thermal insulation capacity of FPC. In order to explore this technology, this paper describes the results of an experiment that determined the thermal protective performance of FPC with SAF under wood crib fire conditions. We also performed an experiment using FPC materials without SAF and compared the results. Finally, we compared the thermal decomposition of commercial thermal liner material and silica aerogel. The results demonstrate that the thermal performance of SAF bedded sample is better than that without. The maximum temperature difference was about 20 °C. The thermal performance of SAF bedded sample increased with increasing the SAF thick. Additionally, the thermal stability of silica aerogel is good, which can reduce the risk of thermal decomposition during high temperatures.

Keywords: firefighter's protective clothing, silica aerogel felt, thermal protective performance, wood crib fire, thermal gravimetric analysis.

1. INTRODUCTION

Firefighters wear personal protective equipment during firefighting that is primarily designed to provide a degree of heat protection from the thermal environment for the upper and lower trunk, neck, arms, and legs [1]. In recent decades, several firefighters have been injured due to fire exposure, highlighting the critical importance of improving the thermal insulation performance of firefighters' protective clothing (FPC) [2, 3]. In general, the thermal insulation performance of FPC is determined by several factors including air gaps, moisture, and stored energy degradation [4–6]. Researchers have explored heat transfer and other factors that impact thermal insulation performance and comfort, and they have applied multiple methods to evaluate the performance of FPC [7–9]. In addition, some researchers have concentrated on improving the thermal protection of FPC by using high-performance nanomaterials [10–13]. Silica aerogel is a nanostructured, porous material with several unique properties including low density (3 kg/m^3), a low thermal insulation value (0.005 W/mK), high specific surface area ($500000\text{--}1200000 \text{ m}^2/\text{kg}$), and high porosity (80–99.8 %) [14, 15].

Other researchers have focused on embedding aerogel in FPC in order to access the potential benefits of improved heat protection and thermal protective performance [16]. Shaid et al. [17] evaluated the thermophysiological comfort of silica aerogel nanoparticle-incorporated wool-Aramid blended fabric, which is used for FPC. They found that the silica aerogel coating has a positive impact on moisture transportation and the overall moisture management property of the fabric. Qi et al. [18] studied the feasibility of using aerogel in FPC to improve

its thermal protective performance. They concluded that incorporating aerogel in FPC can simultaneously improve its TPP and lessen its weight. Lu et al. [19, 20] studied the influence of thermal barrier construction on the level of thermal protection and examined the possibility of incorporating aerogels into thermal barriers to enhance protective performance. They concluded that multilayer nonwoven fabrics treated with aerogels exhibit higher thermal protective performance. Li et al. [21] developed a new type of high-temperature multilayer insulation (MLI) material through a felting process that used alumina silicate fiberpaper and silica fiber net as substrates and hydrophobic silica aerogel granules as filling. They analyzed the relationship between the quantity of filling in the glue and the thermal conductivity coefficient, demonstrating that the lowest thermal conductivity coefficient occurs when the ratio of hydrophobic silica aerogel granules to glue is 2:40. However, very few studies are related to the thermal performance of silica aerogel felt (SAF) bedded FPC under actual fire conditions.

This study concentrates on the possibility of incorporating silica aerogel felt (SAF) into FPC, and the consequences during actual fire exposure. Several large-scale experiments were conducted with SAF bedded in FPC specimens. The samples were exposed to a wood crib fire to simulate an actual fire situation. The results from samples with bedded SAF were compared with those from standard FPC specimens. To further understand the possibility of applying SAF in FPC, thermal gravimetric analyses were conducted for both silica aerogel and commercial thermal liner material. Furthermore, the pyrolysis process in commercial thermal liner material was compared with that in silica aerogel to provide additional insight into the effectiveness of adding SAF to FPC. This study aims to advance understanding of this new

* Corresponding author. Tel.: +86-571-18857174982; fax: +86-571-87676226. E-mail address: dmhuang@cjlu.edu.cn (D. Huang)

technology by investigating the potential benefits of using SAF in FPC.

2. EXPERIMENTAL SETUP

This study applied the ISO9705 Full-Scale Room Fire Test for Surface Products, with slight modifications. This method was chosen for several reasons: The ISO9705 test is an internationally recognized standard, test data was readily available, and a full-scale testing facility was accessible. The ISO9705 instrument is illustrated in Fig. 1 a and b. The internal dimensions of the room were set according to the ISO 9705 standard of 240 cm × 360 cm × 240 cm, with a doorway of 80 cm × 200 cm. The floor of the enclosure was raised 35 cm above the ground. A round hole measuring 60 cm in diameter was located on the 240 cm × 360 cm side, 10 cm above the floor and 30 cm from the left wall.

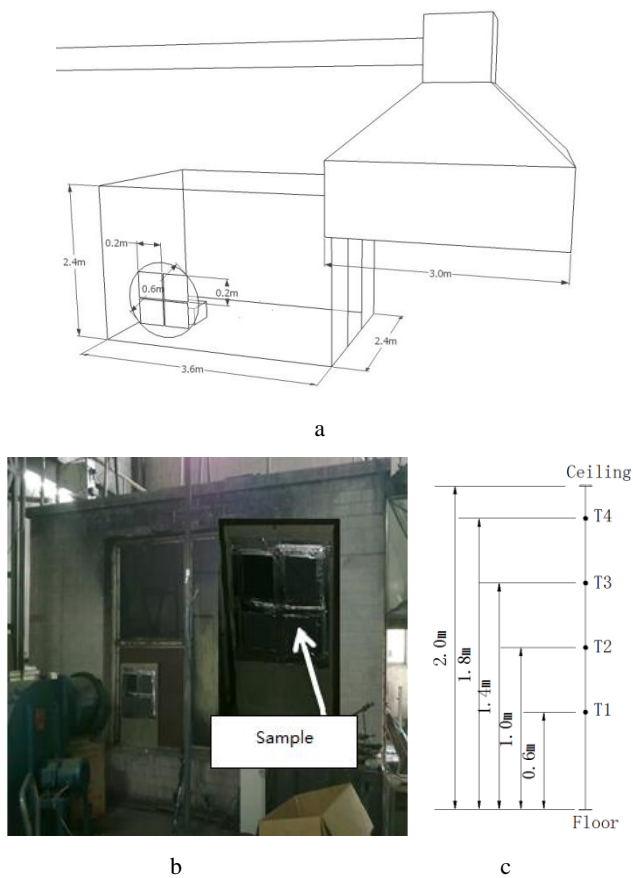


Fig. 1. a – experimental setup; b – ISO9705 full-scale room photo; c – thermocouple tree on the center line of the room

The samples were fixed in place using a holder attached to the hole in the wall. The holder was made of insulation board that was 3 mm thick, 65 cm wide, and 120 cm high, with four 20 cm × 20 cm sections removed from the center to provide exposure areas for the FPC test specimens. The face of the insulation board in the inner room and the areas around each specimen outside the room were covered in aluminum foil to minimize heat transfer from combustion to the insulation board.

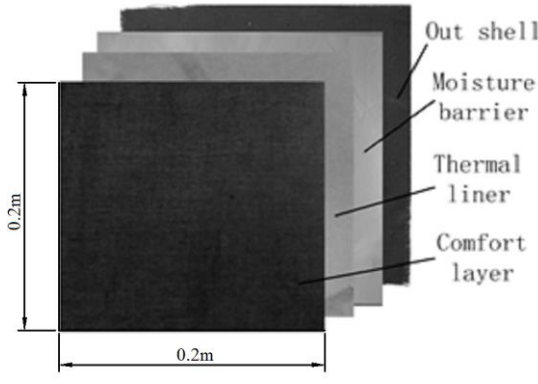
For fuel, the test used a 0.4 m × 0.4 m × 0.32 m wood rib made from 0.4 m × 0.02 m × 0.02 m clear (knot-free)

pine sticks with 10 % water content. Eight layers consisting of ten sticks each were arranged uniformly. Adjacent layers of sticks were set perpendicular to each other. Using the calculation methods in reference [22], the porosity factor, exposed surface, and total cross-sectional area of the wood crib were identified as 0.065 m², 2.344 m², and 0.28 m², respectively. The wood crib was ignited by 100 mL n-heptane.

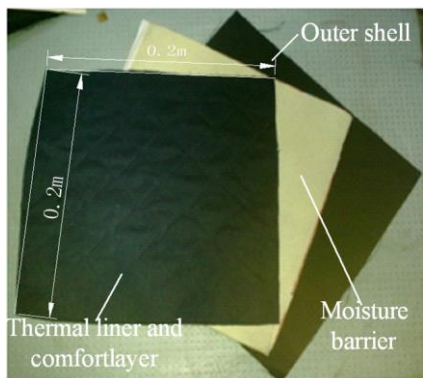
Four 1 mm diameter K-type thermocouples numbered T1 through T4 were used to obtain temperature data on the center line of the door, as seen in Fig. 1 c. Each thermocouple recorded the temperature every second. The temperature field of the FPC on the ambient side surface was monitored by an infrared radiation (IR) thermal imaging camera (Product number: RESEARCH-N1) with a sample rate of 25 times per second. A high-accuracy camera was placed 2 m behind the door to capture the combustion process in the room.

The FPC samples had dimensions of approximately 200 mm × 200 mm, and each sample consisted of four layers: the outer shell, moisture barrier, thermal liner, and comfort layer (see Fig. 2 a).

The outer shell, made of XDB602, functioned as protection against heat and physical shock. The XDB602 is made by transverse and vertical aramid fiber woven together. The moisture barrier consisted of aramid fabric coated with polytetrafluoroethylene film [23]. The aramid fabric usually less than 0.1 mm and it made by the aramid fabric pressed together. The thermal liner was made of aramid insulation felt, with the purpose of protecting the body from heat. The aramid insulation felt is usually very thick and there is large number of pores distributed in it. The density of the material is usually very low. Finally, the comfort layer was made of flame-retardant cotton fabric intended to increase the wearer's comfort. It made by flame retardant cotton woven together. This is a layer of material with absorbent function due to wicking behavior of cotton. The materials in each layer were produced by Shengou Group Co., Ltd., China. Special FPC structures such as fluorescence bands, pockets, and seams were not included in the samples. In actual condition, the thermal liner and comfort layer are stitched together and combined with moisture barrier to form an ensemble. The outer shell is a single layer. The samples were placed in a test chamber with a constant temperature of 30 °C and ambient humidity of 60 % for 24 h before the experiment. The outer shell and moisture barrier layer were the same for all specimens, while the thermal liner was replaced in different samples by SAF layers of different thicknesses. The outside of each specimen was covered in aluminum foil to secure each layer and minimize heat transfer to the insulation board, as seen in Fig. 2 b. In addition, to shed additional light on the thermal decomposition process of silica aerogel and thermal liner material, thermal gravimetric analyses of those materials were conducted. The dynamic degradation was conducted in a thermobalance (DTG-60, Shimadzu) from 20°C to 1000°C at a rate of 20°C/min. Sample masses of 1.3 mg and 6.8 mg of silica aerogel and aramid insulation felt, respectively, were subjected to thermal degradation. The time interval for recording mass losses in the samples was 1 s.



a



b



c

Fig. 2. The structure of the sample for: a—each layer of FPC; b—the structure of each layer in actual use; c—structure of specimen

3. RESULTS AND DISCUSSION

3.1. Fire test

In this study, a full-scale fire test was performed to explore the effect on thermal protection performance of adding SAF to FPC materials. The pre-made wood cribs were kept in a humidity chamber with a relative humidity of 55 % and a temperature of 23.2°C for two weeks. Fig. 3 shows a series of images of the test at various times. The photos show that the fire was associated with higher ventilation values; the flames remained attached to the crib as in free burn and burned quite vigorously. The wood crib fire was a stereo fire, in that both the outer surface and interior burned simultaneously due to the hollowness of the structure.



50s 150s 600s 1000s

Fig. 3. Fire process in the burning room

A thermocouple tree was set at the center line of the combustion room door. The temperature at various heights was recorded every 1 s. Fig. 4 shows the temperature profiles over time. The data show that the temperature increased with increasing height. The temperature curves at T4 and T3 are quite different, suggesting that the bottom of the smoke layer was located between T4 and T3 inside the test room. A stabilization phase occurred between 1300 s and 2200 s due to the stable combustion of the wood crib. Fig. 4 also shows that temperatures at positions T1 and T2 remained near the ambient value. The maximum temperatures at positions T1, T2, and T3 were lower than that at the T4 point due to the radiation of ash after the flame out.

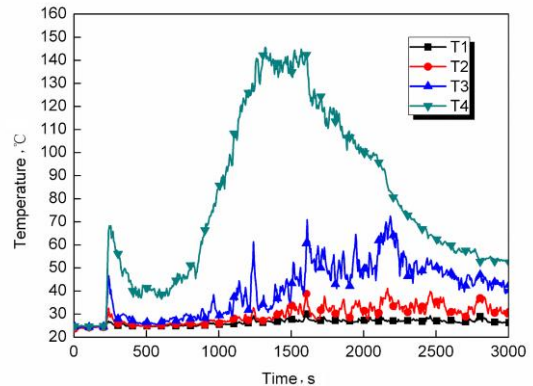


Fig. 4. Temperature vs time at the center line of the door

3.2. Fire protective performance

This experiment investigated the thermal protective performances of multilayer FPC materials with and without SAF by measuring the temperature of the comfort layer surface under the influence of a wood crib fire. SAF thicknesses of 3 mm, 6 mm, and 10 mm were considered. During the experiment, no visible post-exposure damage was observed at the outer shell, SAF, or comfort layer. The color of the outer shell layer changed from navy blue to brown and it is no longer flexibility and easy to be break for the virgin FPC materials. For the samples added SAF, the outer shell layer is still flexibility and it is not

significant difference when the SAF thickness changes from 3 mm to 10 mm.

For the moisture barrier layer made by PTFE film, it has been carbonized with a large number of cracks on the surface for the virgin FPC materials. When the SAF added, the moisture barrier displayed discoloration, and off-gassing was also observed during heat exposure, but the color become lighter as the SAF thickness increase. These phenomena indicate material degradation. The thermal liner also displayed discoloration both for the virgin and replaced SAF materials and the color become lighter as the SAF thickness increase. The color of the comfort layer of the virgin FPC material changed to dark brown, while for the samples added SAF, it almost as the same as the one didn't exposure to heat.

For performance comparison, the experiment measured the transient temperature distributions on the comfort layer surfaces for different samples. Fig. 5 shows a typical image sequence of the comfort layers' surface temperatures. The sample at point P1 was the commercial multilayer FPC material, with three layers of thermal liner. The total thermal liner thickness of this specimen was 2.58 mm, close the thickness of the thinnest SAF sample. The samples at points P2, P3, and P4 were multilayer materials in which the thermal liner was replaced with SAF thicknesses of 3 mm, 6 mm, and 10 mm, respectively. The temperatures on the outer surfaces of the four samples on the room side were assumed to be equal because the four specimens were in close proximity to one another.

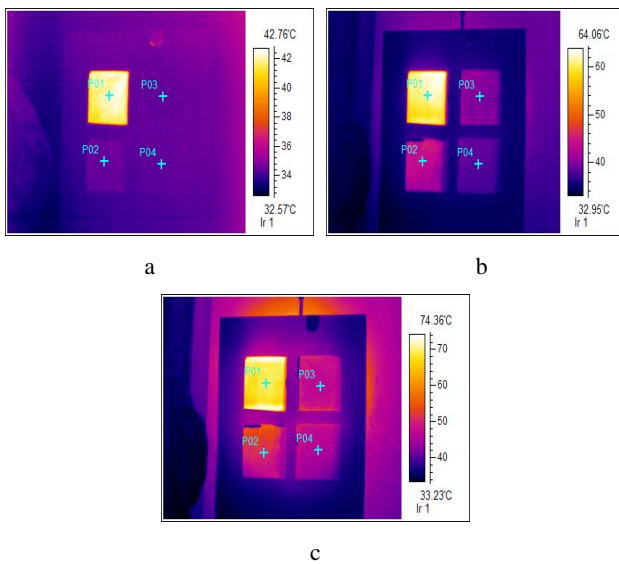


Fig. 5. IR image sequence of the comfort layer surface temperatures: a – 100 s; b – 500 s; c – 2000 s

The measurement area of each sample, as indicated by the solid lines in Fig. 1 a, was about 400 cm^2 . During the experiment, a significant temperature difference was recorded between the comfort layer surface of the FPC material and those of the SAF multilayer materials. At the same time, the temperature on the surface of each individual sample's comfort layer remained quite uniform. As the IR images show, the temperature on the surface of the FPC material's comfort layer was always higher than those of the materials with added SAF, implying that the thermal performance of SAF is superior to that of the

thermal liner material commonly used in FPC. The temperatures of the comfort layer surfaces were measured at the center of each sample, with point P1 being the measurement point for the FPC sample, and points P2, P3, and P4 being the measurement points for the SAF-supplemented samples. Fig. 6 compares the temperature variations at the four comfort layer locations.

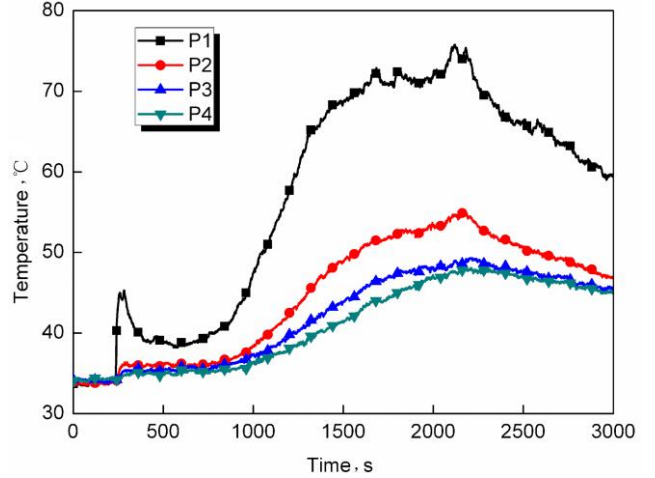


Fig. 6. Temperature on the back surface of the comfort layer

Fig. 6 shows that the temperature at point P1 was always much higher than the temperatures at the other points at the same time. Furthermore, the temperature appears to jump about 10°C at about 200 s, decreasing immediately afterwards. This pattern is due to the use of n-heptane as the sole ignition fuel. When the n-heptane was exhausted, the wood crib was still at the initial stage of burning, and the temperature was therefore relatively low. The temperatures at points P2, P3, and P4 remained almost the same for the first 900 s. Then, the temperature at point P2 began to increase more quickly than those at points P3 and P4; this implies that under conditions of fire, the thermal protective performance of SAF increases as its thickness increases. It shows that the maximum temperatures at points P1 through P4 were approximately 75°C , 50°C , 47°C , and 46°C , respectively; all of these temperatures occurred at 2200 s. This may be because the ash left by the burned wood crib continued heating the room after the flame went out.

The temperature differences between point P1 and the other points can be divided into two phases: the stabilization phase, which occurred between 1300 s and 2200 s, and the destabilization phase, which occurred after 2200 s. These phases are analogous to heating and cooling phases. The maximum temperature differences between point P1 and the points P2, P3, and P4 were 20°C , 25°C , and 28°C , respectively, implying that SAF performs better than commercial thermal liner material of the same thickness. These results also indicate that increasing the thickness of SAF has little effect on its thermal performance. The curve showing the temperature difference between points P1 and P4 almost overlaps with that of points P1 and P3 during the destabilization phase, suggesting that the temperatures on the comfort layer surfaces of materials with 6 mm and 10 mm of SAF were

almost the same. During the experiments which replaced thermal liner by SAF, the structure integrity of outer shell material was not broken. But for the initial material, we can see some cracks in the outer shell layer and it complete destruction when we bend it. This phenomenon also appears in other layers. That is to say the thermal insulation performance of silica aerogel is better than that of the thermal liner materials, which is in good agree with the results indicated by Lu and Li [19, 20].

As discussed above, replacing traditional FPC thermal liner with SAF can significantly increase the thermal protective performance of FPC under fire conditions. SAF owes its excellent insulation properties to its small pore size (10–100 nm), as shown in Fig. 7. Fig. 7 b is the microscopic image of silica aerogel, which is observed in a high-resolution field emission SEM (JSM-5610LV, JEOL Co. Ltd, Japan). The magnification is 50 kX. The thermal conductivity of silica aerogel is extremely low due to its structure. The main heat transfer mechanisms of aerogel are heat conduction through the silica skeleton and gas radiation through pores. Convection is usually negligible in silica aerogel, due to the material's tiny pore size [24–26].

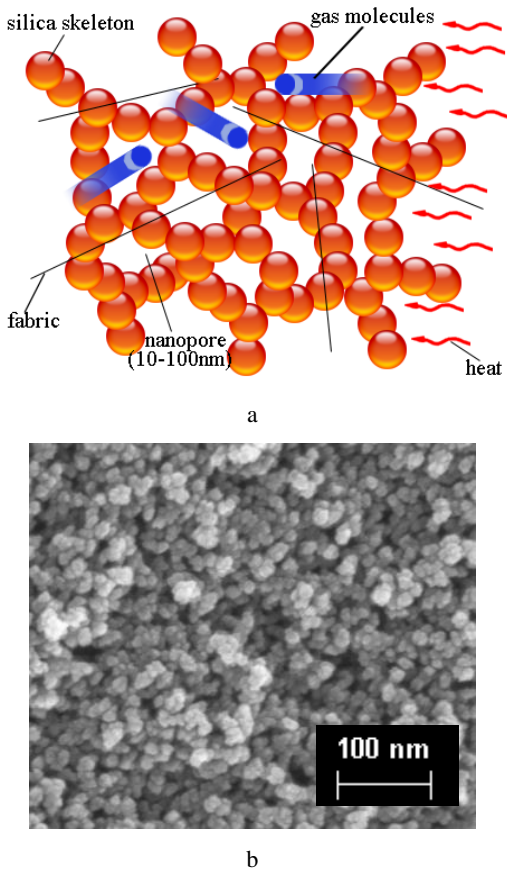


Fig. 7. a – nanostructure of SAF; b – microscopic image of silica aerogel

According to the first law of Fourier, energy transport by conduction is proportional to the thermal conductivity and inversely proportional to the distance. As mentioned above, the thermal performance of SAF bedded FPC is better than that without. And it increases with increasing SAF thick. This is possibly due to the difference of thermal conductivity. The thermal conductivity of SAF and thermal

liner material is $0.03 \text{ W m}^{-1} \text{ K}^{-1}$ and $0.05 \text{ W m}^{-1} \text{ K}^{-1}$, respectively. Therefore, more energy transport from outer shell layer to the inner layer through thermal liner than that of SAF at the same thick. The maximum temperature of P1 and P2 is about 75 °C and 52 °C, respectively.

3.3. Thermogravimetric analysis

The pyrolysis characteristics of silica aerogel and aramid insulation felt were measured as the temperature rose from 20 °C to 1000 °C at a rate of 10 °C/min under air conditions. Fig. 8 shows the pyrolysis curves for silica aerogel and thermal liner material. Based on the shape of the curves, four phases can be identified in the aramid insulation felt sample: a water evaporation phase before 220 °C; a fast pyrolysis phase between 220 °C and 280 °C, in which approximately 30 % of the sample was lost; an intermediate pyrolysis phase between 280 °C and 530 °C, in which approximately 43 % of the sample was lost; and a slow pyrolysis phase above 530 °C. For silica aerogel, thermal decomposition occurred between 300 °C and 600 °C, and the sample's total mass loss was about 9 %. These results suggest that using SAF in FPC can reduce thermal liner material decomposition, preventing harm to firefighters during firefighting.

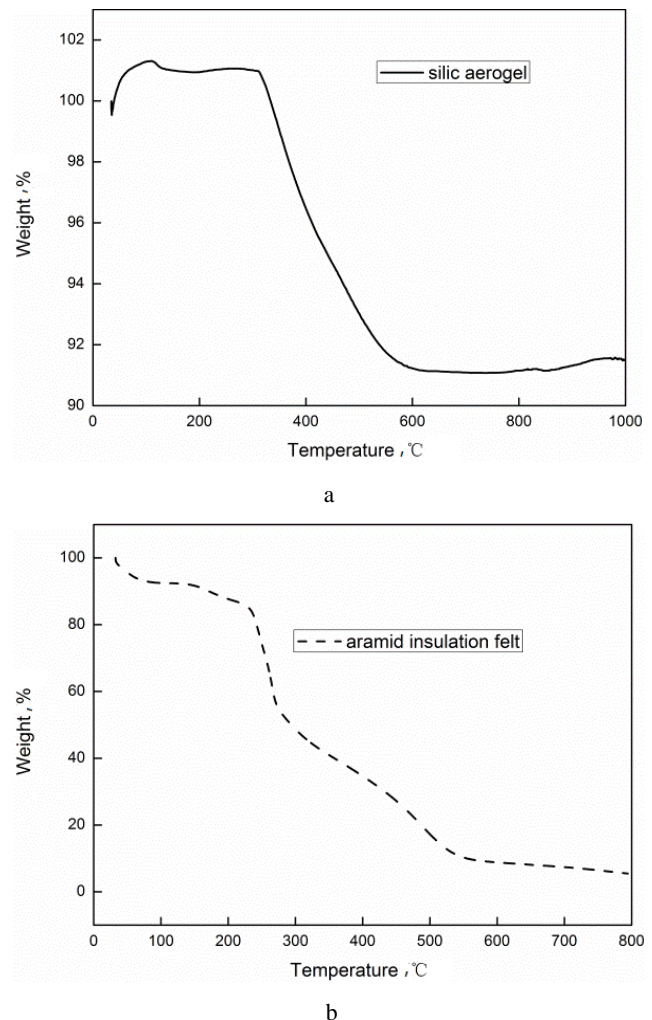


Fig. 8. Pyrolysis curves of silica aerogel and thermal liner material in TGA: a – silica aerogel; b – aramid insulation felt

Furthermore, silica aerogel has an ultralow density that can reach 3 kg/m^3 . The density of traditional thermal liner material is usually 80 kg/m^3 . Therefore, using silica aerogel in FPC can decrease the total weight of FPC and alleviate the burden on firefighters.

4. CONCLUSIONS

This study involved a large-scale experiment with a wood crib fire in order to measure the thermal protective performance of FPC materials with and without SAF. The experiment simulated realistic firefighting conditions through heat transmission on exposure to flame. Additionally, thermal gravimetric analyses of silica aerogel and thermal liner material were conducted. Based on our findings, we can draw the following conclusions:

1. The thermal performance of SAF bedded sample is better than that without. The maximum temperature difference between the specimens with and without SAF was 20°C during the stable combustion phase.
2. The thermal performance of SAF bedded sample increase with increasing SAF thickness. But the temperature on the surface of the comfort layer decreased with it. The decrease was very minor when the SAF thickness exceeded 6 mm, especially during the heating and cooling phases. An optimal thickness of SAF should be identified for use in FPC.
3. The degree of thermal decomposition resulting from pyrolysis was associated with the properties of the sample. The total mass loss of commercial thermal liner material was significantly larger than that of silica aerogel. In thermal liner material, pyrolysis apparently takes place through pyrolytic decomposition beginning at 200°C ; in silica aerogel, decomposition begins at 300°C .

Acknowledgments

This work was supported by the National Natural Science Foundation of China, No.51306168, Zhejiang Provincial Natural Science Foundation, China, No. LY17E060004, Key Laboratory of Furniture Inspection Technology of Zhejiang Province, No. 2016J08.

REFERENCES

1. **The Ministry of Public Security of the People's Republic of China.** Fire Fighting Protective Clothing[S]. in GA10-2002, 2002.
2. **Chitrphiromsri, P., Kuznetsov, A.V.** Modeling Heat and Moisture Transport in Firefighter Protective Clothing During Flash Fire Exposure *Heat and Mass Transfer* 41 (3) 2005: pp. 206–215.
3. **Taylor, N.A.S., Lewis, M.C., Notley, S.R.** A Fractionation of the Physiological Burden of the Personal Protective Equipment Worn by Firefighters *European Journal of Applied Physiology* 112 (8) 2012: pp. 2913–2921.
4. **Zhu, F., Zhang, W., Song, G.** Heat Transfer in a Cylinder Sheathed by Flame-resistant Fabrics Exposed to Convective and Radiant Heat Flux *Fire Safety Journal* 43 (6) 2008: pp. 401–409.
5. **Cui, Z., Zhang, W.** Study of the Effect of Material Assembly on the Moisture and Thermal Protective Performance of Firefighters Clothing *Fibres & Textiles in Eastern Europe* 17 (6) 2009: pp. 80–83.
6. **Eni, E.U.** Developing Test Procedures for Measuring Stored Thermal Energy in Firefighter Protective Clothing, 2005: pp. 13–14.
7. **Zhu, F., Ma, S., Zhang, W.** Study of Skin Model and Geometry Effects on Thermal Performance of Thermal Protective Fabrics *Heat and Mass Transfer* 45 (1) 2008: pp. 99–105.
8. **Barker, R.L., Guerth-Schacher, C., Grimes, R.V., Hamouda, H.** Evaluating the Effects of Moisture on the Thermal performance of Firefighter Protective Clothing in Low Level Heat Exposures *Textile Research Journal* 76 (1) 2006: pp. 27–31.
9. **Mercer, G.N., Sidhu, H.S.A.** Theoretical Investigation into Phase Change Clothing Benefits for Firefighters under Extreme Conditions *Chemical Product and Process Modeling* 4 (3) 2009: pp. 1–12.
10. **Turaga, U., Singh, V., Lalagiri, M., Kiekens, P., Ramkumar, S.S.** Nanomaterials for Defense Applications [M]// Intelligent Textiles and Clothing for Ballistic and NBC Protection. Springer Netherlands, 2012: pp. 197–218.
11. **Sundararajan, S., Chandrasekaran, A.R., Ramakrishna, S.** An Update on Nanomaterials-Based Textiles for Protection and Decontamination *Journal of the American Ceramic Society* 93 (12) 2010: pp. 3955–3975.
12. **Song, K., Zhang, Y., Meng, J., Emily, C., Tajaddod, N., Li, H., Minus, M.L.** Structural Polymer-based Carbon Nanotube Composite Fibers: Understanding the Processing–structure–performance Relationship *Materials* 6 2013: pp. 2543–2577.
13. **Porter, D., Metcalfe, E., Thomas, M.** Nanocomposite Fire Retardants—A review *Fire and Materials* 24 (1) 2000: pp. 45–52.
[https://doi.org/10.1002/\(SICI\)1099-1018\(200001/02\)24:1<45::AID-FAM719>3.0.CO;2-S](https://doi.org/10.1002/(SICI)1099-1018(200001/02)24:1<45::AID-FAM719>3.0.CO;2-S)
14. **Dorcheh, A.S., Abbasi, M.H.** Silica Aerogel: Synthesis, Properties and Characterization *Journal of Materials Processing Technology* 199 (1) 2008: pp. 10–26.
<https://doi.org/10.1016/j.jmatprotec.2007.10.060>
15. **Dai, S., Ju, Y.H., Gao, H.J., Lin, J.S., Pennycook, S.J., Barnes, C.E.** Preparation of Silica Aerogel using Ionic Liquids as Solvents *Chemical Communications* 3 2000: pp. 243–244.
16. **Chakraborty, S., Pisal, A.A., Kothari, V.K., Rao, A.V.** Synthesis and Characterization of Fibre Reinforced Silica Aerogel Blankets for Thermal Protection *Advances in Materials Science and Engineering* 2016: pp. 1–8.
17. **Shaid, A., Furgusson, M., Wang, L.** Thermophysiological Comfort Analysis of Aerogel Nanoparticle Incorporated Fabric for Fire Fighter's Protective Clothing *Chemical and Materials Engineering* 2 (2) 2014: pp. 37–43.
18. **Qi, Z., Huang, D., He, S., Yang, H., Hu, Y., Li, L.M., Zhang, H.P.** Thermal Protective Performance of Aerogel Embedded Firefighter's Protective Clothing *Journal of Engineered Fibers and Fabrics* 2 (8) 2013: pp. 134–139.
19. **Lu, J., Hong, K.A., Do, N.H., Yoon, K.J.** Effect of Thermal Barrier on Thermal Protective Performance of Firefighter Garments *Journal of Fiber Bioengineering and Informatics* 4 (3) 2011: pp. 245–252.
20. **Lu, J., Hong, K.A., Yoon, K.** Effect of Aerogel on Thermal Protective Performance of Firefighter Clothing

- Journal of Fiber Bioengineering and Informatics* 6 (2) 2013: pp. 315–324.
<https://doi.org/10.3993/jfbi09201309>
21. **Li, J., He, F., He, X.** New-type High-Temperature Multilayer Insulation Material *Materials Science and Technology* 4 2009: pp. 531-534.
 22. **Xu, Q., Griffin, G., Jiang, Y., Preston, C., Bicknell, A.D., Bradbury, G.P., White, N.** Study of Burning Behavior of Small Scale Wood Crib with Cone Calorimeter *Journal of Thermal Analysis and Calorimetry* 91 (3) 2007: pp. 787–790.
 23. **Zhou, L., Meng, J.** Current Situation and Development of Waterproof and Moisture Permeable Fabric *Progress Text Science Technology* 1 2010: pp. 38–39.
 24. **Xie, T., He, Y.L., Hu, Z.J.** Theoretical Study on Thermal Conductivities of Silica Aerogel Composite Insulating Material *International Journal of Heat and Mass Transfer* 58 (1) 2013: pp. 540–552.
 25. **Zhao, J.J., Duan, Y.Y., Wang, X.D., Wanga, B.X.** Radiative Properties and Heat Transfer Tharacteristics of Fiber-loaded Silica Aerogel Composites for Thermal Insulation *International Journal of Heat and Mass Transfer* 55 (19) 2012: pp. 5196–5204.
 26. **Wei, G., Liu, Y., Zhang, X., Yu, F., Du, X.** Thermal Conductivities Study on Silica Aerogel and its Composite Insulation Materials *International Journal of Heat and Mass Transfer* 54 (11) 2011: pp. 2355–2366.
<https://doi.org/10.1016/j.ijheatmasstransfer.2011.02.026>